# Collective excitations of Dirac electrons in a graphene layer with spin-orbit interaction

X.F. Wang and Tapash Chakraborty
*Department of Physics and Astronomy, The University of Manitoba, Winnipeg, Canada, R3T 2N2*

Coulomb screening and excitation spectra of electrons in a graphene layer with spin-orbit interaction (SOI) is studied in the random phase approximation. The SOI opens a gap between the valence and conduction bands of the semi-metal Dirac system and reshapes the bottom and top of the bands. As a result, we have observed a dramatic change in the long-wavelength dielectric function of the system. An undamped plasmon mode emerges from the inter-band electron-hole excitation continuum edge and vanishes or merges with a Landau damped mode on the edge of the intra-band electron-hole continuum. The characteristic collective excitation of the Dirac gas is recovered in a system with a high carrier density.

PACS numbers: 71.10.-w,75.10.Lp,75.70.Ak,71.70.Gm

Since the recent discovery of quantum Hall effect in graphene [1, 2, 3], there has been an upsurge of interest in understanding its electronic properties. Graphene has a promising potential for nanoscale device applications [4] and is also very interesting physically because of its unusual Dirac-Weyl type band-structure near the Fermi level [5, 6, 7, 8, 9, 10, 11]. As a single layer of graphite or an unrolled single-walled nanotube, the energy band structure of graphene is well known just as for the graphite or for a nanotube [5, 6, 8]. The past few years have also evidenced increased activities in the role of spin-orbit interaction (SOI) in nanostructures because it introduces many unusual features in these systems. The SOI is also found to exhibit interesting effects such as the spin Hall effect in graphene [8] but overall its effect in graphene is as yet, unclear [12]. Further, the electron-electron interaction is important to understand the behavior of electrons in graphene and has been studied by many authors in graphite-based structures but without the SOI included [12, 13, 14, 15]. In this letter, we explore the effect of SOI on the electron-electron interaction and the characteristic excitations in a graphene layer.

Graphene has a honeycomb lattice of carbon atoms with two sublattices. Its energy band can be calculated by the tight-binding model [5, 6] and an intrinsic graphene is a semimetal with the Fermi energy located at the inequivalent $K$ and $K'$ points at opposite corners of its hexagonal Brillouin zone [5]. In the effective mass approximation, the Hamiltonian of electrons near the Fermi energy is expressed by a $8\times 8$ matrix. Since the SOI due to the atomic potential only mixes the states corresponding to the two sublattices, we can reduce the matrix to four independent $2\times 2$ blocks. In the representation of the two sublattices, the Hamiltonian of a spin-up electron near the $K$ point of the reciprocal space reads [8, 9]

$$H = v\boldsymbol{p}\cdot\boldsymbol{\sigma} + \Delta_{so}\sigma_z = \begin{bmatrix} \Delta_{so} & -i\hbar v\nabla^- \\ -i\hbar v\nabla^+ & -\Delta_{so} \end{bmatrix}, \quad (1)$$

with $\boldsymbol{\sigma} = (\sigma_x, \sigma_y, \sigma_z)$ the Pauli matrices in the pseudospin space of the two sublattices and $\nabla^{\pm} = \partial/\partial x \pm i\partial/\partial y$. Here $\Delta_{so}$ is the strength of the spin-orbit interaction (SOI) and $v = 10^6$ m/s is the 'light' velocity of the Dirac electron gas. The eigenfunctions are, $\Psi^+_{\boldsymbol{k}}(\boldsymbol{r}) = e^{i\boldsymbol{k}\cdot\boldsymbol{r}}\begin{pmatrix}\cos(\alpha_{\boldsymbol{k}}/2)\\ e^{i\phi_{\boldsymbol{k}}}\sin(\alpha_{\boldsymbol{k}}/2)\end{pmatrix}$ for the state $|\boldsymbol{k},+\rangle$ in the conduction band of energy $E^+_{\boldsymbol{k}} = \sqrt{\Delta^2_{so}+\hbar^2v^2k^2}$ while $\Psi^-_{\boldsymbol{k}}(\boldsymbol{r}) = e^{i\boldsymbol{k}\cdot\boldsymbol{r}}\begin{pmatrix}\sin(\alpha_{\boldsymbol{k}}/2)\\ -e^{i\phi_{\boldsymbol{k}}}\cos(\alpha_{\boldsymbol{k}}/2)\end{pmatrix}$ for the state $|\boldsymbol{k},-\rangle$ in the valence band $E^-_{\boldsymbol{k}} = -\sqrt{\Delta^2_{so}+\hbar^2v^2k^2}$ with $\tan\phi_{\boldsymbol{k}} = k_y/k_x$, $\tan\alpha_{\boldsymbol{k}} = \hbar vk/\Delta_{so}$, and $k = \sqrt{k_x^2+k_y^2}$. For a bare Coulomb scattering of two electrons at states $|\boldsymbol{k},\lambda\rangle$ and $|\boldsymbol{p},\lambda_1\rangle$ into states $|\boldsymbol{k}+\boldsymbol{q},\lambda'\rangle$ and $|\boldsymbol{p}-\boldsymbol{q},\lambda_1'\rangle$ respectively, the interaction matrix elements are

$$v^{\lambda,\lambda',\lambda_1,\lambda_1'}_{\boldsymbol{k},\boldsymbol{p}} = g^{\lambda,\lambda'}_{\boldsymbol{k}}(\boldsymbol{q})v_0(q)g^{\lambda_1,\lambda_1'}_{\boldsymbol{p}}(-\boldsymbol{q}). \quad (2)$$

Here $v_0 = e^2/(2\epsilon_0\epsilon_i q)$ is the two-dimensional Coulomb interaction (in Fourier space) with the high-frequency dielectric constant $\epsilon_i = 1$ [11], $g^{\lambda,\lambda'}_{\boldsymbol{k}}(\boldsymbol{q})$ is the interaction vertex, and the index $\lambda = \pm$ denotes the two bands. It is straightforward to show that the RPA dressed interaction matrix elements have the same form as the bare interaction matrix elements, i.e. Eq. (2) [16]. As a result, the dielectric matrix is expressed as a unit matrix multiplied by a dielectric function

$$\hat{\epsilon}(q,\omega) = 1 - v_0(q)\hat{\Pi}(\mathbf{q},\omega) \quad (3)$$

with the electron-hole propagator

$$\hat{\Pi}(\mathbf{q},\omega) = 4\sum_{\lambda,\lambda',\boldsymbol{k}} |g^{\lambda,\lambda'}_{\boldsymbol{k}}(\boldsymbol{q})|^2 \frac{f[E^{\lambda'}_{\boldsymbol{k}+\boldsymbol{q}}] - f[E^{\lambda}_{\boldsymbol{k}}]}{\hbar\omega + E^{\lambda'}_{\boldsymbol{k}+\boldsymbol{q}} - E^{\lambda}_{\boldsymbol{k}} + i\delta}. \quad (4)$$

The factor 4 comes from the degenerate two spins and two valleys at $K$ and $K'$; and the vertex factor reads $|g^{\lambda,\lambda'}_{\boldsymbol{k}}(\boldsymbol{q})|^2 = [1 + \lambda\lambda'\cos\alpha_{\boldsymbol{k}+\boldsymbol{q}}\cos\alpha_{\boldsymbol{k}} + \lambda\lambda'\sin\alpha_{\boldsymbol{k}+\boldsymbol{q}}\sin\alpha_{\boldsymbol{k}}(k+q\cos\theta)/|\boldsymbol{k}+\boldsymbol{q}|]/2$ with $\theta$ being the angle between $\boldsymbol{k}$ and $\boldsymbol{q}$. Since the intra-band backward scattering at $\boldsymbol{q} = 2\boldsymbol{k}$ and the inter-band vertical transition at $\boldsymbol{q} = 0$ are not allowed under Coulomb interaction in the system, we have $|g^{\lambda,-\lambda}_{\boldsymbol{k}}(0)|^2 = |g^{\lambda,\lambda}_{\boldsymbol{k}}(2\boldsymbol{k})|^2 = 0$.

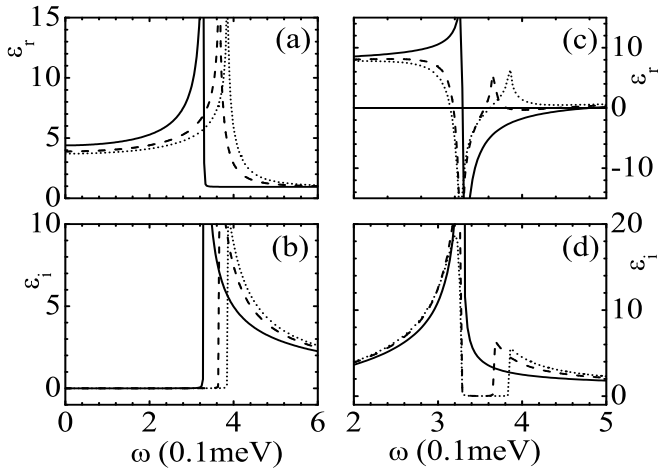


FIG. 1: Real ($\epsilon_r$) and imaginary ($\epsilon_i$) parts of the dielectric function vs $\omega$ at $T = 0$ (left panels) and $T = 2$ K (right panels) for an intrinsic graphene ($E_F = 0$) and the SOI strength $\Delta_{so} = 0$ (solid), 0.08 meV (dashed), and 0.1 meV (dotted). The wave vector is $q = 0.05 \times 10^5$ cm$^{-1}$.

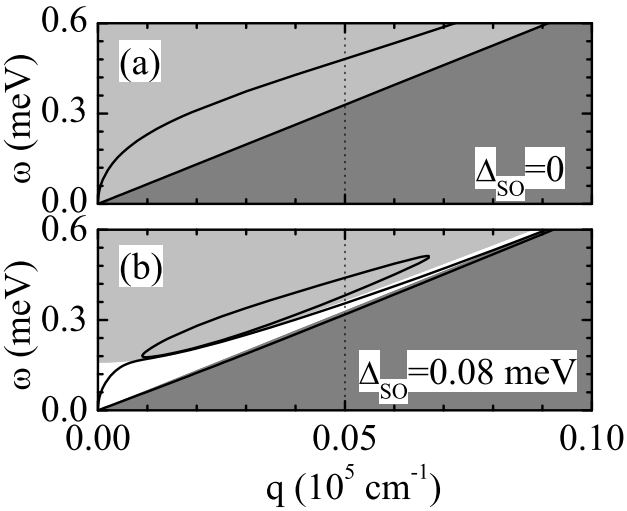


FIG. 2: Plasmon spectrum (thick curves) of an electron gas in an intrinsic graphene ($E_F = 0$) at $T = 2$ K with $\Delta_{so} = 0$ in (a) and 0.08 meV in (b). Intra- (dark shaded) and inter- (light shaded) band single-particle continuums are also shown. The vertical dotted lines indicate the $q$ values for which the dielectric function is shown in Fig. 1 (c).

The collective excitation spectrum is obtained by finding the zeros of the real part of the dielectric function $\epsilon_r$. For convenience we denote each zero as a plasmon mode which may differ from the convention used in other places where some Landau damped modes are not counted since they do not have poles for $\hat{\epsilon}^{-1}$.

First we explore the properties of an intrinsic graphene where the net electron density is equal to zero and $E_F = 0$. In Fig. 1 (a) and (b), we show the real ($\epsilon_r$) and imaginary ($\epsilon_i$) parts of the dielectric function at $T = 0$ for different SOI strengths [6, 8] $\Delta_{so} = 0$ (solid), 0.08 (dashed), and 0.1 meV (dotted) at a wave vector $q = 0.05 \times 10^5$ cm$^{-1}$. In the absence of the SOI, i.e. for $\Delta_{so} = 0$, the zero temperature electron-hole propagator is given by $\hat{\Pi}_0(\mathbf{q}, \omega) = -q^2/[4\sqrt{v^2q^2 - \omega^2}]$, which has been previously obtained via the renormalization group theory [10, 13]. We have $\epsilon_r = 1$ (for $\omega > vq$) above the inter-band electron-hole continuum (EHC) edge and $\epsilon_i = 0$ (for $\omega < vq$) below it since only the interband transition is allowed for electrons. With an increasing $\Delta_{so}$, the peaks of $\epsilon_r$ and $\epsilon_i$, which are located at the edge of the inter-band EHC, $\omega_H = 2\sqrt{\Delta_{so}^2 + \hbar^2 v^2 q^2/4}$, shift to higher energies. At the same time, for $\omega > \omega_H$, $\epsilon_r$ increases continuously with $\Delta_{so}$. In the intrinsic graphene there is no plasmon mode at the zero temperature.

At a finite temperature, the intra-band transition is allowed and contributes to the electron-hole propagator of Eq. (4) while the inter-band contribution is reduced from that at zero temperature because of the electronic occupation of the conduction band. For $\Delta_{so} = 0$ where $\omega_L = \omega_H$, a $\epsilon_r$ dip at the intra-band EHC edge $\omega_L = vq$ in the high energy side is formed as shown by the solid curve in Fig. 1 (c) and two roots of the equation $\epsilon_r = 0$ or two plasmon modes may appear, one at $\omega = vq$ while the other has a higher energy. In Fig. 1 (d), we observe a finite value of $\epsilon_i$ for $\omega < \omega_L$ due to the intra-band transition and a reduced $\epsilon_i$ for $\omega > \omega_L$ corresponding to the weakening of inter-band scattering as the temperature increases. As a result, the plasmon mode at $vq$ is strongly damped while the other is weakly damped. With increasing $\Delta_{so}$, the $\epsilon_r$ peak due to inter-band transitions shifts with $\omega_H$ to a higher energy while the $\epsilon_r$ dip of intra-band transitions stays with $\omega_L$. Since the $\epsilon_r$ peak has a lower energy than the $\epsilon_r$ dip initially at $\Delta_{so} = 0$, the peak and the dip will merge at first and split again. As a result, the $\epsilon_r$ curve is deformed in such a way that two extra zeros of $\epsilon_r$ or two new plasmon modes emerge at a finite $\Delta_{so}$. If $\Delta_{so}$ is further increased the $\epsilon_r$ peak finally disappears as the gap between the $\epsilon_r$ dip and peak becomes wider and the inter-band interaction diminishes. Corresponding to the separation of the $\epsilon_r$ peak from its dip, the $\epsilon_i$ curve develops a gap between $\omega_L$ and $\omega_H$ [Fig. 1 (d)].

The $\omega$ versus $q$ spectrum of the plasmon modes at $T = 2$ K is plotted by thick solid curves for $\Delta_{so} = 0$ in Fig. 2 (a) and $\Delta_{so} = 0.08$ meV in Fig. 2 (b). We observe one strongly Landau-damped plasmon mode at $\omega = vq$ and a weakly damped one in the inter-band EHC with an approximate dispersion of $\omega \propto \sqrt{q}$ near $q = 0$ in the $\Delta_{so} = 0$ case. A finite $\Delta_{so}$ separates $\omega_H$ from $\omega_L$ and opens a gap between the intra- and inter-band EHC's. Near $q = 0$ the former weakly damped plasmon mode becomes undamped because it is now located in the gap. Due to a strong inter-band single-particle transition at the edge of the inter-band EHC, the dispersion curve of this mode is squeezed to a lower energy when it approaches the inter-band EHC edge and then splits into three plasmon modes, i.e., two new plasmon modes emerge near the inter-band EHC edge. One of

the modes remain undamped in the EHC gap (or the $\epsilon_i$ gap) while the other two are located inside the inter-band EHC. The latter two modes merge and disappear at $q$ near $0.07 \times 10^5$ cm$^{-1}$ in Fig. 2 (b). The undamped mode survives in larger wavevectors until it merges with the strongly damped mode at the intra-band EHC edge.

As explained in Fig. 1 (c), the emergence of undamped and extra plasmon modes is a direct result of the SOI in the graphene system, which opens a EHC gap and separates the $\epsilon_r$ peak attributed to inter-band transitions from the $\epsilon_r$ dip attributed to intra-band transitions. The plasmon spectrum is a result of the interplay between the intra- and inter-band contributions to the dielectric function and may change significantly as parameters of the system such as the temperature and the electron density vary as discussed in the following.

By applying a gate voltage to a graphene layer, one can control the electron density and the Fermi energy in the system [1, 2] and it is interesting to see the corresponding change in the excitations. Due to the symmetry of the band structure, systems having the same density of electrons or holes are equivalent. Here we consider a system with a net electron density and positive Fermi energy $E_F$. For a Dirac gas in a graphene without a SOI, the extra electrons in the conduction band reduce the inter-band scattering rate but enhances the intra-band scattering by increasing the length of the Fermi ring. At $T = 0$, a EHC gap of width $2v(k_F - q)$ is opened above the intra-band EHC edge in the range $0 < q < k_F$. For $E_F > \Delta_{so}$ the $\epsilon_r$ has a dip in the higher energy side of $\omega = vq$ and a diminished peak in the lower energy side similar to the case of $E_F = 0$ but for $T > 0$ [Fig. 1 (c)]. As for the corresponding $\epsilon_i$, the peak in the higher energy side at $\omega = vq + 0^+$ is flattened because the inter-band transition to the bottom of the conduction band is forbidden but a new peak appears in the other side at $\omega = vq - 0^+$ due to the now allowed intra-band transition. As a result of the $\epsilon_r$ dip at $\omega = vq + 0^+$ introduced by the intra-band transition, a Landau damped plasmon mode appears near $\omega = vq$ and another one above, with an approximate dispersion $\omega \propto \sqrt{q}$ at the small $q$. As compared to the spectrum of an intrinsic graphene at a finite temperature [Fig. 2 (a)], here the latter mode is undamped near $q = 0$ and has a flatter dispersion slope near the crossing of the dispersion curve and the inter-band EHC edge. Instead of an emergence of the new plasmon modes when the plasmon dispersion curve exits the EHC gap of SOI the plasmon dispersion smoothly exits the EHC gap corresponding to a finite Fermi energy.

In the presence of the SOI, the physical scenario changes from the $\Delta_{so} = 0$ case for long-wavelength excitations if the Fermi energy is located near the SOI gap. In Fig. 3, we plot the dielectric function versus $\omega$ for different Fermi energies at $T = 0$ (left panels) and $T = 2$ K (right panels) in a graphene with the SOI strength of $\Delta_{so} = 0.08$ meV. The dashed curves of Fig. 1 for the $E_F = 0$ case is also plotted here for comparison. At $T = 0$, due to modification of the energy bands at

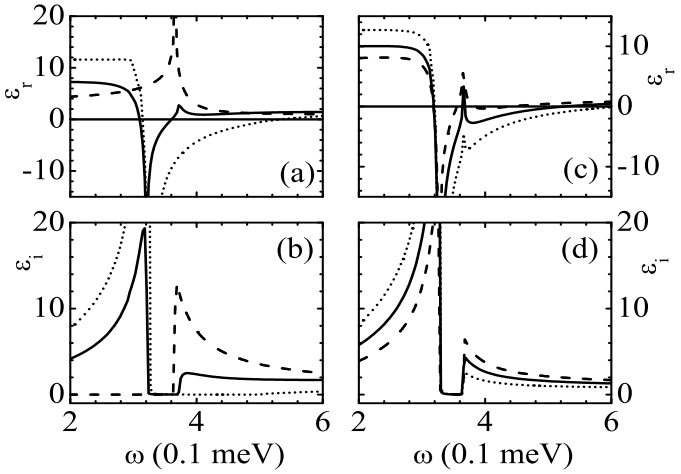


FIG. 3: Real ($\epsilon_r$) and imaginary ($\epsilon_i$) parts of the dielectric function vs $\omega$ at $T = 0$ (left panels) and $T = 2$ K (right panels) in a graphene of $\Delta_{so} = 0.08$ meV with $E_F = 0$ (dashed), 0.25 meV (solid), and 0.4 meV (dotted). $q = 0.05 \times 10^5$ cm$^{-1}$.

the bottom (or top), the intra-band EHC edge deviates from $\omega = vq$ to a lower energy $\sqrt{\Delta_{so}^2 + \hbar^2 v^2 (k_F + q)^2} - \sqrt{\Delta_{so}^2 + \hbar^2 v^2 k_F^2}$ for small $q$. In Fig. 3 (a) and (b), we observe a shift of the $\epsilon_r$ dip and of the edge of the lower $\epsilon_i$ peak to an energy lower than $vq$ for the $E_F = 0.25$ meV curve (solid). With the Fermi energy inside the conduction band, the inter-band EHC edge at $T = 0$ is expressed by $\omega_H$ when $q > 2k_F$ but shifts to a higher energy $\sqrt{\Delta_{so}^2 + \hbar^2 v^2 k_F^2} + \sqrt{\Delta_{so}^2 + \hbar^2 v^2 (k_F - q)^2}$ for $q < 2k_F$. As a result, the solid $\epsilon_r$ peak and the upper $\epsilon_i$ gap edge ($k_F = 0.036$ cm$^{-1}$) have higher energies than the dashed ones ($k_F = 0$) in Fig. 3 (a) and (b). When the Fermi energy becomes higher, for example, as shown by the dotted curve of $E_F = 0.4$ meV in Fig. 3 (a) and (b), the system reverts to the Dirac gas and the dielectric function becomes similar to that in the $\Delta_{so} = 0$ case. From the solid curve for $\epsilon_r$ in Fig. 3 (a) we observe that the SOI shifts the inter-band $\epsilon_r$ peak to a higher energy and can change the weakly damped plasmon mode inside the inter-band EHC to an undamped mode in the EHC gap created by the SOI.

At a finite temperature, however, the restriction to single-particle transitions by the Fermi energy is relaxed and both the intra- and inter-band EHC edges are the same as those for $E_F = 0$. In Fig. 3 (c), where $\epsilon_r$ at $T = 2$ K is shown, the peaks and the dips of all the curves have the same energy and $\epsilon_i$ for different Fermi energies in Fig. 3 (d) have the same gap. These characteristics of the single-particle excitation continuum edges are also shown in Fig. 4 by the light and dark shades for inter- and intra-band EHC's respectively.

The effect of SOI on the zero-temperature plasmon spectrum of a graphene with a finite Fermi energy outlined in Fig. 2 (a) is illustrated by its dispersion in Fig. 4 (a). At a wavevector $q$ close to or higher than $k_F$, strong

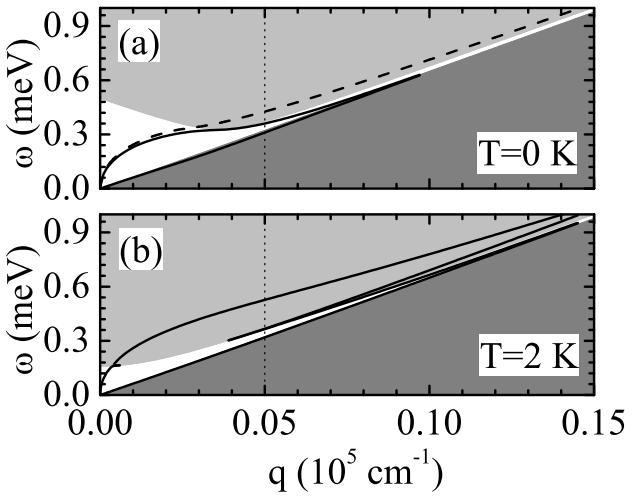


FIG. 4: The same as in Fig. 2 but with $E_F = 0.25$ meV at $T = 0$ (a) and $T = 2$ K (b). The solid curves are for $\Delta_{so} = 0.08$ meV and the dashed in (a) for $\Delta_{so} = 0$. The corresponding dielectric functions for the values of $q$ indicated by the vertical dotted lines are given in Fig. 3 by the solid curves.

inter-band transitions between states of similar pseudospin $|\boldsymbol{k}, +\rangle$ and $|\boldsymbol{k}', -\rangle$ with $\boldsymbol{k}$ anti-parallel to $\boldsymbol{k}'$ are possible. The contribution of these transitions at a finite $\Delta_{so}$ increases the real part of the dielectric function at high energies and moves one zero of $\epsilon_r$ to a lower energy. As a result, the corresponding plasmon dispersion curve is excluded from the inter-band EHC and confined in the EHC gap opened by the finite Fermi energy and the SOI. At a finite temperature $T = 2K$, the electrons spread to higher energies and the inter-band transition rate is reduced at large $q$ but increased at a small $q$. In this case, the dispersion curve of the mode above $vq$ remains almost intact except a splitting to three modes when it enters the inter-band EHC near $q \simeq 0.004 \times 10^5$ cm$^{-1}$ as shown in Fig. 4 (b). Being different from the behavior exhibited in Fig. 2 (b), here the two extra plasmon modes along $\omega_H$ merge with each other soon after the splitting and emerge again at a higher $q$.

In summary, we have derived the electron-hole propagator and the dynamically screened Coulomb interaction matrix of an electron system in graphene with spin-orbit interaction in the random phase approximation, using the standard and widely used technique for multicomponent systems. In a system of intrinsic graphene without the SOI, our result reduces to the analytical result of a Dirac electron gas previously obtained by the renormalization group theory. The spin-orbit interaction changes the Dirac gas semimetal to a narrow gap semiconductor system. The carriers far from the gap remain as the Dirac type while those near the gap shows different characteristics. At a finite temperature, the SOI splits the inter-band single-particle continuum from the intra band one and an undamped plasmon mode exists in the gap of the single-particle excitation spectrum. For a gap of 0.16 meV, this plasmon mode exists in a range of wave vector of the order of $0.1\times10^5$cm $^{-1}$, which could perhaps be observed in experiments. With net electrons or holes in a graphene, a plasmon mode above the intra-band single-particle continuum exists and the Coulomb interaction is screened at a high energy even at the zero temperature. The SOI may push this mode to the single-particle continuum gap or split it into three modes. In contrast to the negligible effect of SOI to the dynamic Coulomb screening and the plasmon spectrum of a Fermi gas in a InGaAs quantum well [17], the SOI may change significantly these properties of a Dirac gas in a graphene.

One of the authors (X.F.W) thanks P. Vasilopoulos for helpful discussions. The work has been supported by the Canada Research Chair Program and a Canadian Foundation for Innovation (CFI) Grant.

[‡] Electronic address: tapash@physics.umanitoba.ca

[1] K.S. Novoselov, et al., Nature **438**, 197 (2005).
[2] Y. Zhang, Y.W. Tan, H.L. Stormer, and P. Kim, Nature **438**, 201 (2005).
[3] Y. Zhang, et al., Phys. Rev. Lett. **96**, 136806 (2006).
[4] M. Wilson, Phys. Today **59** (1), 21 (2006).
[5] P.R. Wallace, Phys. Rev. **71**, 622 (1947); J.C. Slonczewski and P. R. Weiss, *ibid.* **109**, 272 (1958); A. Zunger, Phys. Rev. B **17**, 626 (1978).
[6] T. Ando, in *Nano-physics & Bio-electronics: A new Odyssey*, T. Chakraborty, F. Peeters, U. Sivan, (eds.), (Elsevier, Amsterdam, New York, 2002), Ch. 1.
[7] G.W. Semenoff, Phys. Rev. Lett. **53**, 2449 (1984); F.D.M. Haldane, *ibid.* **61**, 2015 (1988).
[8] C.L. Kane and E.J. Mele, Phys. Rev. Lett. **95**, 226801 (2005); D.P. DiVincenzo and E.J. Mele, Phys. Rev. B **29**, 1685 (1984).
[9] N.A. Sinitsym, J.E. Hill, H. Min, J. Sinova, and A. H. MacDonald, cond-mat/0602598.
[10] D. V. Khveshchenko, cond-mat/0604180.
[11] N. M.R. Peres, F. Guinea, and A.H. Castro Neto, Phys. Rev. **72**, 174406 (2005); J. Nilsson, A.H. Castro Neto, N.M.R. Peres, and F. Guinea, cond-mat/0512360.
[12] T. Ando, J. Phys. Soc. Jpn. **69**, 1757 (2000).
[13] J. González, F. Guinea, M.A.H. Vozmediano, Nucl. Phys. B **424**, 595 (1994); Phys. Rev. B **59**, R2474 (1999); *ibid.* **63**, 134421 (2001).
[14] J.V. Alvarez and G.G.N. Angilella, Solid State Commun. 132, 683 (2004).
[15] O. Vafek, cond-mat/0605642.
[16] B. Vinter, Phys. Rev. B **15**, 3947 (1977).
[17] X. F. Wang, Phys. Rev. B **72**, 85317 (2005).